NANO LETTERS

Letter

pubs.acs.org/NanoLett

Facile Thermal and Optical Ignition of Silicon Nanoparticles and Micron Particles

Sidi Huang, Venkata Sharat Parimi, Sili Deng, Srilakshmi Lingamneni, and Xiaolin Zheng*

Department of Mechanical Engineering, Stanford University, Stanford, California 94305, United States

Supporting Information

ABSTRACT: Silicon (Si) particles are widely utilized as high-capacity electrodes for Li-ion batteries, elements for thermoelectric devices, agents for bioimaging and therapy, and many other applications. However, Si particles can ignite and burn in air at elevated temperatures or under intense illumination. This poses potential safety hazards when handling, storing, and utilizing these particles for those applications. In order to avoid the problem of accidental ignition, it is critical to quantify the ignition properties of Si particles such as their sizes and porosities. To do so, we first used differential scanning calorimetry to experimentally determine the reaction onset temperature of Si particles under slow heating rates (~0.33 K/s). We found that the reaction onset temperature of Si particles increased with the particle diameter from 805 °C at 20−30 nm to 935 °C at 1−5 μm. Then, we used a xenon (Xe) flash lamp to ignite Si particles under fast heating rates (~10^3 to 10^6 K/s) and measured the minimum ignition radiant fluence (i.e., the radiant energy per unit surface area of Si particle beds required for ignition). We found that the measured minimum ignition radiant fluence decreased with decreasing Si particle size and was most sensitive to the porosity of the Si particle bed. These trends for the Xe flash ignition experiments were also confirmed by our one-dimensional unsteady simulation to model the heat transfer process. The quantitative information on Si particle ignition included in this Letter will guide the safe handling, storage, and utilization of Si particles for diverse applications and prevent unwanted fire hazards.

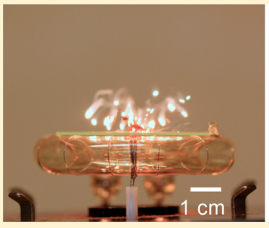

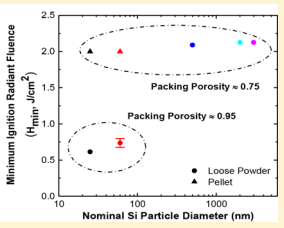

KEYWORDS: *Silicon nanoparticles, flash ignition, energetic materials, ignition, combustion, fire hazard*

Silicon (Si) particles, ranging from nanoparticles to micron-sized particles, are promising material candidates for high-capacity electrodes for Li-ion batteries,[1] elements for thermoelectric devices,[2,3] agents for hydrogen generation,[4] bioimaging, and therapy,[5] components for single electron tunneling,[6] elements for supporting bioelectric interfaces,[7] and many other applications. Si particles, with a high volumetric energy density (75.9 kJ/cm^3),[8] can ignite and burn energetically in air upon heating or under intense illumination. Hence, safe handling, storage, and utilization of Si particles for such applications require prevention of unwanted ignition and fire hazards. Such requirements call for understanding and quantification of the ignition and combustion properties of Si particles. Some studies have investigated the combustion properties of Si particles with solid oxidizers (e.g., sodium perchlorate and fluorinated compounds), including flame propagation speeds and pressurization rates,[9−11] and found that more intense burning and faster flame propagation are achieved when the size of Si particles decreases from microns to nanometers.[11] One study looked into the ignition properties of micron-sized Si particles in air by electric spark ignition[12] and found that the minimum ignition energy decreased from 2.9 J for 18 μm Si particles to around 0.06 J for 3.6 μm Si particles. Other studies have investigated the ignition properties of porous Si (P−Si), which is crystalline Si containing nanosized pores with hydrogen terminated surfaces.[13] It was found that P−Si composites have low ignition temperatures[14] and can be optically ignited in air by a low power xenon (Xe) flash (<1 J/cm^2) through the photothermal effect.[13] To date, there is no quantitative information on the ignition properties of Si particles in air as a function of particle sizes and porosity.

In this work, we investigated the ignition properties of Si particles of five different sizes, including 20−30 nm (U.S. Research Nanomaterial Inc.), 50−70 nm (U.S. Research Nanomaterial Inc.), 500 nm (Skyspring Nanomaterial Inc.), 1−3 μm (U.S. Research Nanomaterial Inc.), and 1−5 μm (Alfa Aesear Inc.). The morphologies, surface terminations, elemental compositions, and size distribution of these samples are summarized in Tables S1 and S2. In addition, we aim to provide multiple data points in the same size category (20−30 nm vs 50−70 nm Si, and 1−3 μm vs 1−5 μm Si) to cross-check for consistency and accuracy. We did not include larger Si particles since they are not ignitable under our experimental conditions. We quantified the ignition properties of these particles under both slow and fast heating conditions as the intermediate heating rates are difficult to realize and control experimentally. Reaction onset temperatures were measured by differential scanning calorimetry (DSC) at a slow heating rate

Received: April 25, 2017
Revised: August 14, 2017
Published: September 5, 2017

DOI: 10.1021/acs.nanolett.7b01754
Nano Lett. 2017, 17, 5925−5930

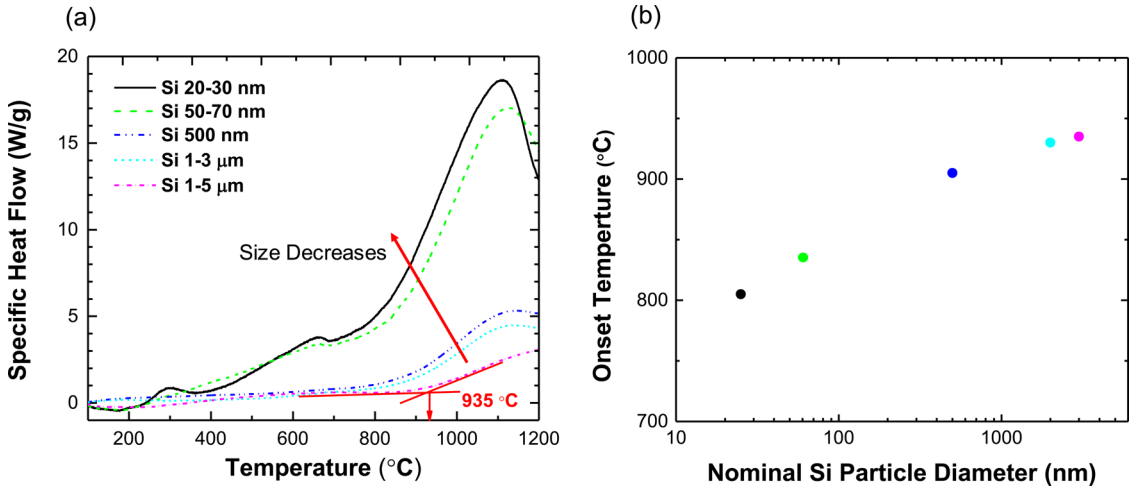

Figure 1. (a) Baseline-corrected DSC traces (normalized by the sample mass) for the oxidation reaction between O_2 and Si particles of different sizes with a heating rate of 0.33 K/s. The reaction onset temperature is defined as the intersection between the largest tangent of the heat flow curve and the extrapolated baseline. (b) Extracted reaction onset temperature of Si particles as a function of their diameters.

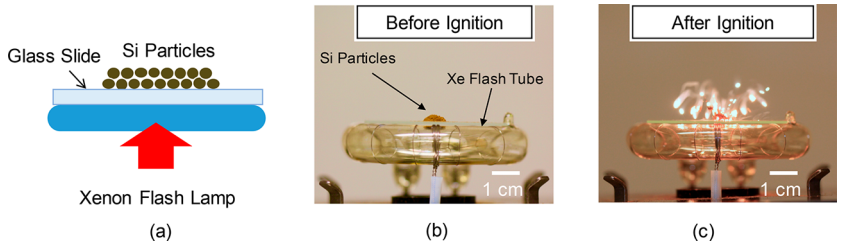

Figure 2. (a) Schematic of the experimental setup for Xe flash ignition. Inset shows the optical image of a Si particle bed. Optical images (b) before and (c) after igniting the Si particles with the flash. Si: 20−30 nm particles at the porosity of around 0.95.

(~0.33 K/s), while minimum ignition radiant fluences were quantified with a Xe flash lamp at a fast heating rate (~10^3 to 10^6 K/s). The heating rate for TGA/DSC experiments is controlled by the tool's furnace and can be varied from 0.1 to 5 K/s.[15] The heating rate for flash ignition experiments is estimated by the lamp power, flash pulse duration (~4 ms) light absorption, and heat transfer properties of the material under consideration. The estimated heating rate is on the order of 10^3−10^6 K/s, which is much faster than the heating rates obtainable in a TGA/DSC.[16] Hence, for comparison, we refer to the TGA/DSC and flash ignition experiments as slow and fast heating rates, respectively. Both heating rates represent different practical applications. The TGA/DSC experiment is a good approximation of slow heating cases, such as ignition on hot plates, ovens, and furnaces. Flash ignition experiments represent situations such as optical ignition, shock ignition, and spark ignition, which result in heating rates of 10^5 K/s or higher.[17,18] For both cases, we investigated the effects of particle size and/or porosity on ignition properties of the particle beds.

We first used the DSC measurement (Setaram Labsys Evo) to determine the reaction onset temperature of Si particles as a function of their size. For a typical measurement, a Si particle powder sample of 10 mg was placed in a 100 μL alumina crucible inside the DSC chamber. The sample was heated from 100 to 1200 °C with a constant heating rate of 0.33 K/s. The heating was conducted with a carrier gas consisting of 80% vol. Ar and 20% vol. O_2 with a total flow rate of 40 sccm. After heating, the sample was cooled down to room temperature and heated again with the same process. The second round heat flow trace was used to correct the baseline of the first round heat flow trace based on the method described previously.[19,20] This baseline correction was applied to all the DSC traces reported here. The baseline correction is necessary because the specific heat capacity of the sample changes as the reactants are converted to products. To minimize the effect of this specific heat capacity change, we subtracted the heat flow for the first run (Si oxidized to SiO_2) by the second run (SiO_2). Figure 1a plots the baseline-corrected DSC traces (normalized by the sample mass) for the oxidation reaction between O_2 and Si particles of different sizes. The DSC traces show that the specific heat flow from the Si oxidation reaction becomes more pronounced over the entire temperature range for smaller Si particles. This increase in the specific heat release reflects that smaller Si particles are oxidized more due to the reduced diffusion length scales. Similar characteristics were also observed previously for the oxidation of nano- and micron-sized aluminum particles.[21,22] To quantitatively illustrate the size effect on the ignition properties of Si particles, we define a reaction onset temperature as the intersection between the largest tangent of the heat flow curve and the extrapolated baseline (Figure 1a). For example, the extracted onset temperature is 935 °C for the 1−5 μm Si particles. The extracted onset temperatures from Figure 1a are plotted in Figure 1b, which shows that increasing the Si particle diameter monotonically increases the onset temperature of Si particles, from ~805 °C for 20−30 nm to 935 °C for 1−5 μm Si particles. The DSC trace of Si nanoparticle (20−30 nm) has two additional peaks at low temperature because about 25 wt % of these particles have sizes less than 20−30 nm (shown in

DOI: 10.1021/acs.nanolett.7b01754
Nano Lett. 2017, 17, 5925−5930

Table S2). Those smaller particles ignite at lower temperatures, leading to the formation of additional small exothermic peaks. These results show that smaller Si particles have lower onset temperature to initiate the oxidation reaction because smaller Si particles have smaller diffusion distance for oxygen atoms and larger specific surface area to react with oxygen.

The above DSC experiments elucidate the oxidation processes of Si particles under steady and slow heating. In many practical scenarios, Si particles are exposed to fast heating conditions, such as optical illumination and sudden temperature rises due to an electrical short-circuit. To simulate such fast heating conditions, we further study the ignition properties of Si particles that are optically ignited by a Xe flash lamp (Figure 2a,b). The Xe flash lamp, upon being triggered, emits a short pulse of energy (~4 ms). Part of the emitted energy is photoabsorbed by a Si particle bed, resulting in a temperature rise. When the peak temperature of the Si particle bed exceeds its ignition temperature, the Si particle bed is ignited and burns subsequently (Figure 2c).[13] Experimentally, a pile of Si particles (5 mg) with an approximate cross section area of 20 mm^2 is placed over a 1 mm thick glass slide that is placed directly on the Xe flash tube (AlienBees B1600) as shown in Figure 2b. During the experiment, we gradually increase the power level of the Xe flash lamp until we observe ignition (Figure 2c), and the corresponding power level is defined as the minimum ignition radiant fluence (H_{min}, J/cm^2), which is the radiant energy received per unit surface area of the Si particle pile. The radiant fluence from the Xe flash tube at different power settings (Figure S1a) was calibrated by measuring the temperature rise of a soot-covered Si substrate that was exposed to the same flash power level using the method reported in previous work.[23,24] In addition, we can assume uniform radiant fluence at the surface of the Si pile, for the diameter of the Si particle pile (4 to 5 mm) is significantly smaller than that of the flash tube (15 mm).

The measured minimum ignition radiant fluence H_{min} is plotted in Figure 3 for piles of Si particles of different diameters, where the error bar represents the standard deviation of the measured values of H_{min}. Figure 3 also indicates the typical porosity (P) of the Si particle pile formed for each Si particle size. H_{min} should depend on P as well since it affects the effective optical absorption coefficient[25] and

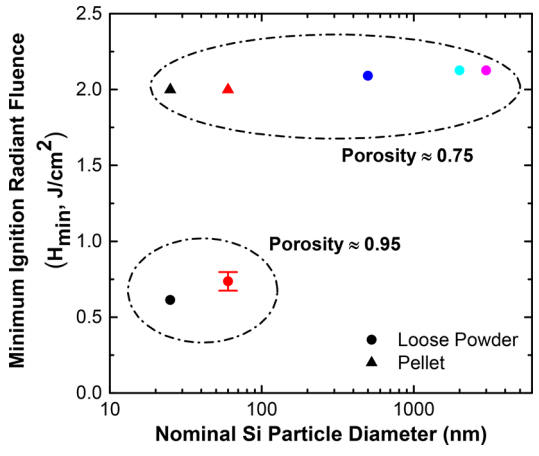

Figure 3. Experimentally measured minimum radiant fluence H_{min} of Si particles as a function of their sizes and porosities. The error bar represents the standard deviation of measured values of H_{min}.

effective thermal conductivity of the pile.[26] The porosity P of the Si particle pile is defined as the volume fraction of air in the pile, and it is evaluated gravimetrically using the following equation:

$$P = 1 - \frac{m_{Si}}{\rho_{Si} V_t} \tag{1}$$

where m_{Si} is the mass of Si particle bed, ρ_{Si} is the density of Si (2.33 g/cm^3), and V_t is the total volume of the Si particle bed. Figure 3 shows that H_{min} increases with increasing the Si particle diameter, similar to the DSC results in Figure 1b. In addition, H_{min} appears to correlate with the porosity as H_{min} is higher for a smaller porosity. To further illustrate the correlation between porosity and H_{min}, we compressed the low porosity piles formed from 20−30 nm Si and 50−70 nm Si particles into pellets (10 mm in diameter by 1 mm thick) to match the porosity (~0.75) of other loose powder samples. We find that for the 20−30 nm Si, H_{min} increased from 0.55 J/cm^2 at porosity of 0.95 to 2 J/cm^2 at porosity of 0.75, indicating that the porosity indeed strongly affects H_{min}.

To understand the dependence of H_{min} on the Si particle size and porosity, we calculated the dynamic temperature profiles inside the Si particle bed using COMSOL Multiphysics software. The computational domain is set up to be similar to the experimental configuration (Figure 2a). As shown in Figure 4a, a 200 μm thick Si particle bed is placed on top of a 1 mm thick glass, and the Xe flash is illuminated from below. The Si particle bed absorbs the flash energy according to the Beer−Lambert law, and the glass slide is assumed to be transparent due to its small optical absorption coefficient. The top part of the Si particle bed loses heat to the ambient air through the convection, and its bottom part loses heat through the conduction to the underneath glass slide. The time-dependent temperature profiles within the Si particle bed are determined by solving the following one-dimensional unsteady heat-transfer equation:

$$(\rho c_p)_{eff} \frac{\partial T}{\partial t} = \frac{\partial}{\partial z}\left(k_{eff}(T)\frac{\partial T}{\partial z}\right) + \alpha_{eff}(1 - R) I_0(t) \exp(-\alpha z) \tag{2}$$

where $(\rho c_p)_{eff}$, k_{eff}, and α_{eff} are the effective heat capacity ($J/(m^3\ K)$), thermal conductivity ($W/(m\ K)$), and absorption coefficient (m^{-1}) at 450 nm for the Si particle/air mixture, R is the reflectivity of the Si particle/air mixture at 450 nm, and $I_0(t)$ is the Xe flash flux density (W/m^2). The initial and boundary conditions are expressed as

$$\text{initial conditions: } T(z, t = 0) = 300\ \text{K}$$

$$\text{boundary conditions: } T(z = -1mm, t) = 300\ \text{K},$$

$$k\frac{\partial T}{\partial t}\bigg|_{z=d} = h(300K - T(d, t))$$

where d is the thickness of the Si particle bed and h is the convective heat transfer coefficient of ambient air and is set to be 10 $W/(m^2\ K)$.[27]

The effective heat capacity $(\rho c_p)_{eff}$ of the Si particle/air mixture is calculated by using the mixture averaged property

$$(\rho c_p(T))_{eff} = (1 - P)\rho_{Si} c_{Si}(T) + P\rho_{air} c_{p,air}(T) \tag{3}$$

where P is the porosity of the Si particle bed, and ρ_{Si}, ρ_{air}, c_{Si}, and $c_{p,air}$ are the density and specific heat capacity of Si and air, respectively. The effective thermal conductivity $k_{eff}(T)$ of the Si

DOI: 10.1021/acs.nanolett.7b01754
Nano Lett. 2017, 17, 5925−5930

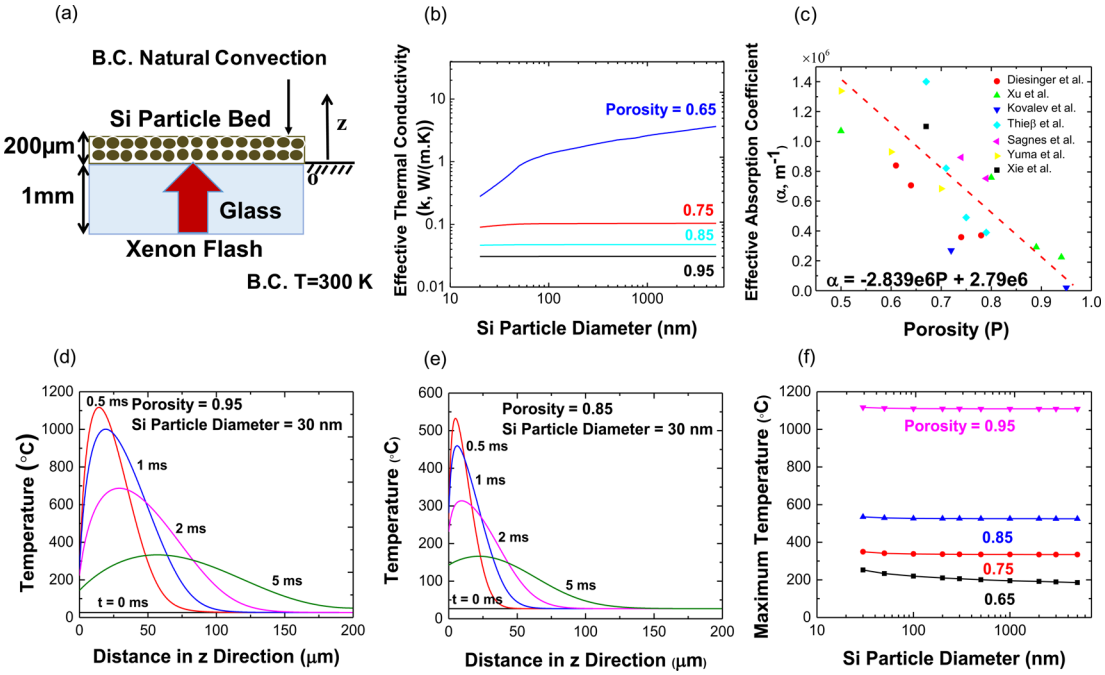

Figure 4. (a) Computational domain and corresponding boundary conditions. (b) Calculated effective thermal conductivity of Si particles at 298 K as a function of particle diameter and porosity. (c) Effective absorption coefficient as a function of porosity. Calculated time-dependent temperature profiles of 30 nm Si particle bed for porosity of (d) 0.95 and (e) 0.85. (f) Extracted maximum temperature within the Si particle bed as a function of their sizes and porosities.

particle/air mixture can be modeled well using the effective medium theory[20] as it accounts for the heterogeneous nature of the mixture and the volume fraction of Si particles in the mixture is within the percolation limit:[28]

$$(1-P)\frac{k_{Si}(T)-k_{eff}(T)}{k_{Si}(T)+2k_{eff}(T)}+P\frac{k_{air}(T)-k_{eff}(T)}{k_{air}(T)+2k_{eff}(T)}=0 \quad (4)$$

where P is the porosity of the Si particle bed, $k_{Si}(T)$ is the size and temperature-dependent thermal conductivity of Si particles,[29,30] and $k_{air}(T)$ is the temperature-dependent thermal conductivity of air.[31,32] The calculated k_{eff} at 298 K is shown in Figure 4b as a function of Si particle size under different porosities. The plot shows that k_{eff} is a strong function of porosity. At low porosity, k_{eff} is higher and shows dependence on the size of Si particles due to the presence of a larger amount of Si particles. In contrast, at high porosity, k_{eff} is lower and shows little dependence on the size of Si particles since the majority of the volume is air. The effective absorption coefficient α_{eff} is assumed to be similar to porous Si films, and the values are extrapolated by linear fitting of the reported absorption coefficients of porous Si[13,25,33−37] (Figure 4c). Here, we assume a constant effective absorption coefficient in our simulation for the following reasons. First, there is limited data in published literature on the size-dependence of the absorption coefficient for Si particles.[38] Second, the purpose of our simulation is to qualitatively identify the controlling parameters that affect the flash ignition behavior. Finally, to demonstrate that the value of the effective absorption coefficient has a very small effect on our simulation, we tested a 20 nm Si particle bed packed at 0.85 and 0.95 porosities and compared the calculated maximum temperature with constant versus size-dependent absorption coefficients. The results show that the difference in T_{max} is less than 5% (Table S3), which does not affect our conclusion. This computation further justifies that our approximation is valid for qualitative comparisons. Similarly, the reflectivity of the Si particle bed at 450 nm was adopted from porous Si film data in the literature.[36] The shape of the Xe flash flux density profile, $I_0(t)$, is experimentally measured using a photodiode (PDA36A, Thorslab) and curve-fitted using MATLAB (Figure S1b). The exact value of $I_0(t)$ in eq 2 for different flash power settings is determined by matching the time integrated value of $I_0(t)$ with the corresponding measured Xe flash radiant fluence (Figure S1a).

Figure 4d,e plots the time-dependent temperature profiles within the Si particle (30 nm in diameter) beds of two different porosities (0.95 and 0.85), both exposed to the same incident Xe flash fluence of 2.15 J/cm^2. Qualitatively, the dynamic temperature profiles are similar for these two porosities. At t = 0 ms (i.e., the initiation point of the flash), the temperature of the Si particle bed is at 300 K everywhere. At t = 0.5 ms, a temperature hot spot appears close to the glass slide because more light absorption occurs near the glass side due to the exponential decay of light absorption with distance.[13] At t = 1 ms, the peak temperature drops due to the decline in the flux density from the Xe flash (Figure S1b), and the simultaneous heat loss to the glass slide and nearby Si particles. At t = 2 and 5 ms, the peak temperature continues to drop, and the overall temperature profile is broadened due to the thermal conduction. Nevertheless, the overall temperature of the Si particle bed is much higher for the higher porosity case (Figure 4d,e). This difference becomes evident when the maximum temperature (T_{max}) that the Si particle bed has reached is plotted in Figure 4f as a function of the Si particle diameter and porosity. Here, we consider the calculated maximum temperature during the flash heating of silicon particle beds (Figure 4f) instead of the onset temperatures from DSC experiments (Figure 1b) due to several reasons. First, the heat transfer and heat loss processes are different between DSC and flash. The Si

DOI: 10.1021/acs.nanolett.7b01754
Nano Lett. 2017, 17, 5925−5930

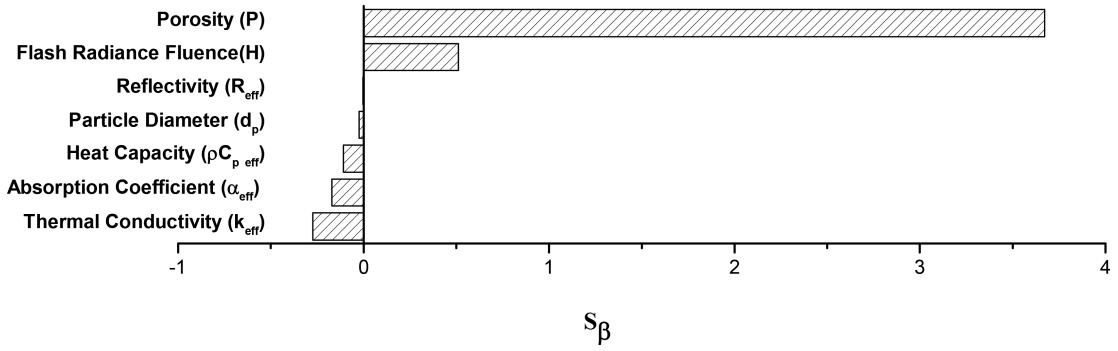

Figure 5. Sensitivity coefficients of various parameters with respect to the maximum temperature that a Si particle bed can achieve. Condition: 30 nm Si particle bed at the porosity of 0.85.

particle bed is nearly isothermal in DSC but has a large temperature gradient during flash ignition, so the ignition temperature will be different in these two cases. Second, our calculated maximum temperature of the silicon bed in Figure 4f is based on a simple model to investigate the controlling factors for flash ignition. Third, our model has a number of approximations, such as using constant light absorption coefficient for the Si particle bed and using effective medium theory to estimate the thermal conductivity. Clearly, the calculated maximum temperature of flash heating of silicon particle beds is quite insensitive to the Si particle diameter but strongly depends on the porosity. Hence, these trends suggest that the porosity, not Si particle size, dominantly affects the optical ignition properties of Si particle beds.

The ignition criteria for flash ignition is that the maximum temperature of the Si particle bed caused by flash photothermal heating, T_{max}, exceeds a certain critical temperature. Thus, the higher the T_{max}, the more likely the particle bed is going to ignite. Hence, to evaluate which parameter affects ignition the most, we numerically calculate the sensitivity coefficient of T_{max} with respect to porosity, flash radiant fluence, effective heat capacity, effective absorption coefficient, and effective thermal conductivity. We define a sensitivity coefficient (S_β) with respect to a parameter β as

$$S_\beta = \frac{\partial \ln T_{max}}{\partial \ln \beta} \quad (5)$$

where T_{max} is the maximum temperature that the Si particle bed can achieve both spatially and temporally, and β are the input parameters in eq 2. The sensitivity analysis was performed for a typical case of 30 nm Si particles packed at a porosity of 0.85, with a flash radiant fluence of 2.15 J/cm^2. Each parameter β is perturbed by 5%, and the new T_{max} was computed, which was used to calculate the corresponding S_β, which is shown in Figure 5. A positive value of S_β means that increasing the value of parameter β will increase T_{max}, which will lower the flash radiant fluence needed for ignition. First, S_P is the largest positive sensitivity coefficient, which implies that ignition is greatly facilitated by increasing the porosity. Second, S_H is also positive, as expected, as increasing the energy provided to Si particles will increase T_{max}. Third, S_{keff} is the largest negative sensitivity coefficient because higher thermal conductivity k_{eff} corresponds to a faster heat diffusion, inhibiting the formation of local hot spots. Fourth, $S_{\alpha eff}$ is also negative, which is counterintuitive. The reason is that higher absorption coefficient α_{eff} means that most light absorption (equivalently heat generation) takes place within a narrower width of the Si particle bed close to the glass slide end, which results in a steeper thermal gradient. The steeper temperature gradient leads to more heat loss to the glass slide and hence generates a negative sensitivity coefficient. Finally, $S_{\rho Cpeff}$ is negative because a larger heat capacity of the Si particle bed will require more heat to raise its temperature.

Conclusion. In summary, the ignition properties of Si nano- and micron-sized particles in air were quantitatively determined under both slow and fast heating rate conditions using DSC and Xe flash ignition tests, respectively. At slow heating conditions, the reaction onset temperature for Si nano- and micron-sized particles is in the range of 800 to 950 °C. Smaller Si particles have a lower onset temperature and release more heat during their oxidation in the TGA/DSC because of their larger specific area and shorter diffusion length scales. At fast heating conditions with a Xe flash lamp, the minimum ignition radiant fluence for Si nano- and micron-sized particles is in the range of 0.6 to 2.2 J/cm^2. The porosity of the Si particle bed, rather than the Si particle size, strongly affects the minimum ignition radiant fluence. This dependence is because higher porosity reduces the effective thermal conductivity, absorption coefficient, and heat capacity. All these factors lead to the formation of hot spots within the Si particle bed, which lead to ignition. In practice, ignition is a complex phenomenon since critical ignition conditions depend on the energy input rate, the heat loss rate from the system to its surroundings, and the heat generation rate from reactions. Nevertheless, since the TGA/DSC experiment is an isothermal experiment, so the onset temperature can be regarded as the minimal temperature needed for ignition. Finally, the fundamental understanding on Si ignition obtained here will be beneficial to safe handling, storing, and utilizing Si particles for diverse applications and preventing unwanted ignition and combustion.

■ ASSOCIATED CONTENT

Supporting Information

The Supporting Information is available free of charge on the ACS Publications website at DOI: 10.1021/acs.nanolett.7b01754.

Measured flash radiant fluence of Xe flash lamp as a function of power setting and the measured flash impulse of Xe flash lamp as a function of time, physical properties of Si particles and maximum temperature of 20 nm Si particles with constant and size-dependent absorption coefficient (PDF)

DOI: 10.1021/acs.nanolett.7b01754
Nano Lett. 2017, 17, 5925−5930

AUTHOR INFORMATION

Corresponding Author

*E-mail: xlzheng@stanford.edu. Phone: +1(650) 736-8953. Fax: +1(650) 723-1748.

ORCID

Sidi Huang: 0000-0001-5703-0807
Sili Deng: 0000-0002-3421-7414
Xiaolin Zheng: 0000-0002-8889-7873

Notes

The authors declare no competing financial interest.

ACKNOWLEDGMENTS

This work was supported by Army Research Office under agreement number W911NF-14-1-0271 and the Office of Naval Research under agreement number N00014-15-1-2028.

REFERENCES

(1) Hwang, T. H.; Lee, Y. M.; Kong, B.-S.; Seo, J.-S.; Choi, J. W. *Nano Lett.* **2012**, *12* (2), 802−807.
(2) Hochbaum, A. I.; Chen, R.; Delgado, R. D.; Liang, W.; Garnett, E. C.; Najarian, M.; Majumdar, A.; Yang, P. *Nature* **2008**, *451* (7175), 163−167.
(3) Boukai, A. I.; Bunimovich, Y.; Tahir-Kheli, J.; Yu, J.-K.; Goddard Iii, W. A.; Heath, J. R. *Nature* **2008**, *451* (7175), 168−171.
(4) Dai, F.; Zai, J.; Yi, R.; Gordin, M. L.; Sohn, H.; Chen, S.; Wang, D. *Nat. Commun.* **2014**, *5*, 3605.
(5) O'Farrell, N.; Houlton, A.; Horrocks, B. R. *Int. J. Nanomedicine* **2006**, *1* (4), 451−472.
(6) Ifuku, T.; Otobe, M.; Itoh, A.; Oda, S. *Jpn. J. Appl. Phys.* **1997**, *36* (6S), 4031.
(7) Jiang, Y.; Carvalho-de-Souza, J. L.; Wong, R. C. S.; Luo, Z.; Isheim, D.; Zuo, X.; Nicholls, A. W.; Jung, I. W.; Yue, J.; Liu, D.-J.; Wang, Y.; De Andrade, V.; Xiao, X.; Navrazhnykh, L.; Weiss, D. E.; Wu, X.; Seidman, D. N.; Bezanilla, F.; Tian, B. *Nat. Mater.* **2016**, *15* (9), 1023−1030.
(8) Auner, N. Silicon as an intermediary between renewable energy and hydrogen. *Deutsche Bank Research*, 2004; Working Paper 11e.
(9) Mason, B. A.; Groven, L. J.; Son, S. F.; Yetter, R. A. *J. Propul. Power* **2013**, *29* (6), 1435−1444.
(10) Thiruvengadathan, R.; Belarde, G. M.; Bezmelnitsyn, A.; Shub, M.; Balas-Hummers, W.; Gangopadhyay, K.; Gangopadhyay, S. *Propellants, Explos., Pyrotech.* **2012**, *37* (3), 359−372.
(11) Terry, B. C.; Lin, Y.-C.; Manukyan, K. V.; Mukasyan, A. S.; Son, S. F.; Groven, L. J. *Propellants, Explos., Pyrotech.* **2014**, *39* (3), 337−347.
(12) Eckhoff, R. K. *J. Electrochem. Soc.* **1986**, *133* (12), 2631.
(13) Ohkura, Y.; Weisse, J. M.; Cai, L.; Zheng, X. *Nano Lett.* **2013**, *13* (11), 5528−5533.
(14) Koch, E.-C.; Clément, D. *Propellants, Explos., Pyrotech.* **2007**, *32* (3), 205−212.
(15) Noor, F.; Zhang, H.; Korakianitis, T.; Wen, D. *Phys. Chem. Chem. Phys.* **2013**, *15* (46), 20176.
(16) Ohkura, Y.; Rao, P. M.; Zheng, X. *Combust. Flame* **2011**, *158* (12), 2544−2548.
(17) Egan, G. C.; Mily, E. J.; Maria, J.-P.; Zachariah, M. R. *J. Phys. Chem. C* **2015**, *119* (35), 20401−20408.
(18) DeLisio, J. B.; Yi, F.; LaVan, D. A.; Zachariah, M. R. *J. Phys. Chem. C* **2017**, *121* (5), 2771−2777.
(19) Parimi, V. S.; Huang, S.; Zheng, X. *Proc. Combust. Inst.* **2017**, *36* (2), 2317−2324.
(20) Stamatis, D.; Jiang, Z.; Hoffmann, V. K.; Schoenitz, M.; Dreizin, E. L. *Combust. Sci. Technol.* **2008**, *181* (1), 97−116.
(21) Sun, J.; Pantoya, M. L.; Simon, S. L. *Thermochim. Acta* **2006**, *444* (2), 117−127.
(22) Mench, M. M.; Kuo, K. K.; Yeh, C. L.; Lu, Y. C. *Combust. Sci. Technol.* **1998**, *135* (1−6), 269−292.
(23) Aslin, H. K. *Rev. Sci. Instrum.* **1967**, *38* (3), 377.
(24) De, N. N.; Cummock, N. R.; Gunduz, I. E.; Tappan, B. C.; Son, S. F. *Combust. Flame* **2016**, *167*, 207−217.
(25) Xie, Y. H.; Hybertsen, M. S.; Wilson, W. L.; Ipri, S. A.; Carver, G. E.; Brown, W. L.; Dons, E.; Weir, B. E.; Kortan, A. R.; Watson, G. P.; Liddle, A. J. *Phys. Rev. B: Condens. Matter Mater. Phys.* **1994**, *49* (8), 5386−5397.
(26) Carson, J. K.; Lovatt, S. J.; Tanner, D. J.; Cleland, A. C. *Int. J. Heat Mass Transfer* **2005**, *48* (11), 2150−2158.
(27) *Thermopedia. A-to-Z Guide to Thermodynamics, Heat and Mass Transfer, and Fluids Engineering*; Begellhouse, 2006; Vol. C.
(28) Garboczi, E. J.; Snyder, K. A.; Douglas, J. F.; Thorpe, M. F. *Phys. Rev. E: Stat. Phys., Plasmas, Fluids, Relat. Interdiscip. Top.* **1995**, *52* (1), 819−828.
(29) Regner, K. T.; Sellan, D. P.; Su, Z.; Amon, C. H.; McGaughey, A. J. H.; Malen, J. A. *Nat. Commun.* **2013**, *4*, 1640.
(30) Glassbrenner, C. J.; Slack, G. A. *Phys. Rev.* **1964**, *134* (4A), A1058−A1069.
(31) Kadoya, K.; Matsunaga, N.; Nagashima, A. *J. Phys. Chem. Ref. Data* **1985**, *14* (4), 947.
(32) Stephan, K.; Laesecke, A. *J. Phys. Chem. Ref. Data* **1985**, *14* (1), 227−234.
(33) Diesinger, H.; Bsiesy, A.; Hérino, R.; Gelloz, B. *Mater. Sci. Eng., B* **2000**, *69−70*, 167−170.
(34) Xu, D.; Guo, G.; Gui, L.; Tang, Y.; Zhang, B. R.; Qin, G. G. *J. Phys. Chem. B* **1999**, *103* (26), 5468−5471.
(35) Kovalev, D.; Polisski, G.; Ben-Chorin, M.; Diener, J.; Koch, F. *J. Appl. Phys.* **1996**, *80* (10), 5978−5983.
(36) Theiß, W. *Surf. Sci. Rep.* **1997**, *29* (3−4), 91−192.
(37) Sagnes, I.; Halimaoui, A.; Vincent, G.; Badoz, P. A. *Appl. Phys. Lett.* **1993**, *62* (10), 1155.
(38) Meier, C.; Gondorf, A.; Lüttjohann, S.; Lorke, A.; Wiggers, H. *J. Appl. Phys.* **2007**, *101* (10), 103112.

DOI: 10.1021/acs.nanolett.7b01754
Nano Lett. 2017, 17, 5925−5930